RSC Medicinal Chemistry

ROYAL SOCIETY OF CHEMISTRY

RESEARCH ARTICLE

View Article Online
View Journal

Cite this: DOI: 10.1039/d0md00162g

Design and synthesis of substituted (1-(benzyl)-1*H*-1,2,3-triazol-4-yl)(piperazin-1-yl)methanone conjugates: study on their apoptosis inducing ability and tubulin polymerization inhibition†

Kesari Lakshmi Manasa,[ab] Sowjanya Thatikonda,[c] Dilep Kumar Sigalapalli,[ab] Sowmya Vuppaladadium,[d] Ganthala Parimala Devi,[a] Chandraiah Godugu,[c] Mallika Alvala,[b] Narayana Nagesh *[d] and Bathini Nagendra Babu *[a]

Received 18th May 2020,
Accepted 29th July 2020

DOI: 10.1039/d0md00162g

rsc.li/medchem

A library of substituted (1-(benzyl)-1*H*-1,2,3-triazol-4-yl)(piperazin-1-yl)methanone derivatives were designed, synthesized and screened for their *in vitro* cytotoxic activity against BT-474, HeLa, MCF-7, NCI-H460 and HaCaT cells by employing 3-(4,5-dimethylthiazol-2-yl)-2,5-diphenyltetrazolium bromide (MTT) assay. Among all the synthesized analogues, compound **10ec** displayed the highest cytotoxicity with the IC_{50} value of 0.99 ± 0.01 μM towards BT-474 cancer cell line. The target compound (**10ec**) was also evaluated for its tubulin polymerization inhibition study. Detailed biological studies such as acridine orange/ethidium bromide (AO/EB), DAPI and annexin V-FITC/propidium iodide staining assay suggested that compound **10ec** induced the apoptosis of BT-474 cells. The clonogenic assay revealed that the inhibition of colony formation in BT-474 cells by **10ec** in concentration-dependent manner. Moreover, the flow cytometric analysis revealed that **10ec** induced apoptosis *via* cell cycle arrest at the sub-G1 and G2/M phase. *In silico* studies of sulfonyl piperazine-integrated triazole conjugates unveil that they possess drug-like properties. According to the molecular modelling studies, compound **10ec** binds to the colchicine binding site of the tubulin.

Introduction

Over the past few decades, 1,2,3-triazole and its derivatives have played a prominent role in the field of medicinal chemistry. The formation of 1,2,3-triazoles using click chemistry has become an efficient method for the preparation of diverse building blocks for chemical synthesis,[1] material and surface science,[2] medicinal chemistry[3] and combinatorial chemistry.[4] Moreover, 1,2,3-triazoles play a noteworthy role among the pharmaceutically important nitrogen-containing heterocyclic scaffolds due to their broad spectrum of biological activities such as anticancer,[5] antitubercular, anticonvulsant,[6] antiallergic,[7] antifungal,[8] antibacterial,[9] antiviral[10] and anti-inflammatory activities.[11] The desirable properties of the 1,2,3-triazole ring, such as hydrogen bonding capability,[12] high dipolar character,[13] rigidity and stability under *in vivo* conditions, are responsible for their enhanced biological properties. Fig. 1 demostrated a biologically important natural products[14] containing the triazole moiety.

It is evident from the literature that sulphonamide-based scaffolds are known to exhibit excellent antibacterial, anticancer, antithyroid, antidiabetic, antiviral and antihypertensive activities. Moreover, piperazine and its derivatives are also important scaffolds. Besides having

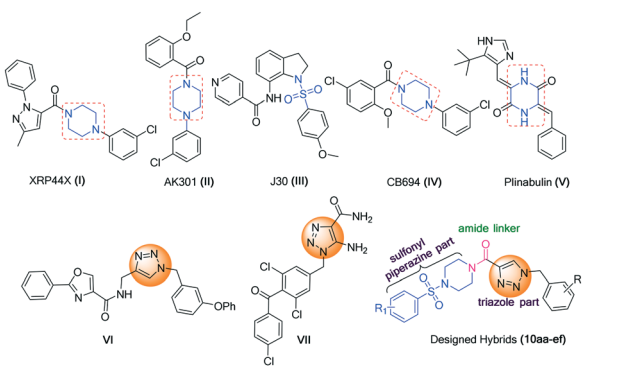

Fig. 1 Chemical structures of a few biologically active sulfonyl piperazine derivatives (**I**–**V**); triazole derivatives (**VI** and **VII**) and designed congeners (**10aa**–**ef**).

[a] *Department of Fluoro-Agrochemicals, CSIR-Indian Institute of Chemical Technology, Hyderabad-500007, India. E-mail: bathini@iict.res.in*
[b] *Department of Medicinal Chemistry, National Institute of Pharmaceutical Education and Research, Hyderabad-500037, India*
[c] *Department of Regulatory Toxicology, National Institute of Pharmaceutical Education and Research (NIPER), Hyderabad-500037, India*
[d] *CSIR-Centre for Cellular and Molecular Biology, Hyderabad 500007, India*

† Electronic supplementary information (ESI) available. See DOI: 10.1039/d0md00162g

antibacterial activity, they also possess potent anticancer properties. AK301 was able to possess a potent ability to hinder the mitosis and induce cell apoptosis.[15] Chopra *et al.*[16] reported piperazine-based colchicine binding site inhibitors, such as XRP44X (Fig. 1). CB694, a piperazine containing compound binds to the colchicine binding site and inhibits the tubulin with an IC_{50} value of 2.3 μM.[17]

Plinabulin[18] showed the effective inhibition of tubulin polymerization at the nanomolar scale. Herein, the sulphonamide scaffold containing the piperazine group was introduced into the triazole nucleus (Fig. 2) and these heterocyclic scaffolds may display a synergistic effect on antitumor activity.

In the recent scenario of drug discovery, more efficient antitumor compounds can be designed by mimicking two or more structural domains into a single framework.[19] Ample amount of literature survey reveals that to date enough efforts have not been made to combine 1,2,3-triazole and sulphonamide moieties into a single molecular scaffold. As a part of the continued research for the development of new antitumor agents, we have designed bifunctional heterocyclic systems containing sulfonyl piperazine-linked 1,2,3-triazole conjugates. In this study, we report the synthesis of substituted (1-(benzyl)-1*H*-1,2,3-triazol-4-yl)(piperazin-1-yl) methanone derivatives (**10aa–ef**), the evaluation of their *in vitro* cytotoxic profile on selected human cancer cell lines and further studies on their mechanistic aspects.

Results and discussion

Chemistry

The synthetic plan was executed as planned and outlined in Scheme 1. The two intermediates substituted benzyl-1,2,3-triazole-4-carboxylic acids (**6a–e**) and substituted sulfonyl piperazine derivatives (**9a–f**) were prepared *via* the conventional methods for the synthesis of desired products. Substituted benzyl-1,2,3-triazole-4-carboxylic acids (**6a–e**) were synthesized from commercially available starting materials. The reaction was employed with different substituted benzyl alcohols (**1a–e**) treated with PBr_3 to give the corresponding benzyl bromides (**2a–e**). We envisioned that the treatment of **2a–e** with sodium azide would result in corresponding benzyl azides (**3a–e**). The key intermediate ethyl 1-benzyl-1*H*-1,2,3-triazole-4-carboxylates (**5a–e**) with different substitutions were synthesized by a standard copper(I) catalyzed azide–alkyne cycloaddition protocol yielding 1,4-adduct from ethyl propiolate (**4**) and **3a–e** by using sodium ascorbate, $CuSO_4{\cdot}5H_2O$, *t*-butanol : H_2O (2 : 1) for 8 h. These were further hydrolyzed in the presence of 4 N NaOH solution to get 1,2,3-triazole acids (**6a–e**) in good yields. Next, a variety of substituted phenyl sulfonyl piperazine intermediates (**9a–f**) were synthesized according to the previous synthetic procedures[20] by the reaction of different substituted benzenesulfonyl chlorides (**7a–f**) with piperazine (**8**) and Et_3N in DCM at 0 °C for 30 min.

Finally, the key intermediate benzyl-1*H*-1,2,3-triazole-4-carboxylic acids (**6a–e**) with different substitution were coupled with **9a–f** using HBTU, HOBt in DMF to afford the desired conjugates **10aa–ef**, and the yields were obtained in the range of 75–90%. All the structures of these conjugates were characterized *via* ^1H and ^{13}C NMR spectroscopy and by HRMS data.

The structure of compound **10aa** could be easily identified by the appearance of a benzylic proton at δ 5.47 ppm and the signals at δ 3.78 and 2.42 ppm, correspond to the methoxy and methyl groups. All the aromatic protons of **10aa** were in the range of δ 7.94–6.79 ppm. Compound **10aa** showed 4 signals at δ 4.42, 3.82, 3.11 and 3.07 ppm, which account for the methylene protons of piperazine. Assessment of ^{13}C NMR of compound **10aa** revealed that the characteristic peak of carbonyl compound is at 158.86 ppm. All the aromatic and aliphatic carbons of the synthesized compounds were in the range of 158.86–20.47 ppm. The HRMS spectra of the designed hybrids showed characteristic $[M + H]^+$ peaks to their corresponding molecular formula.

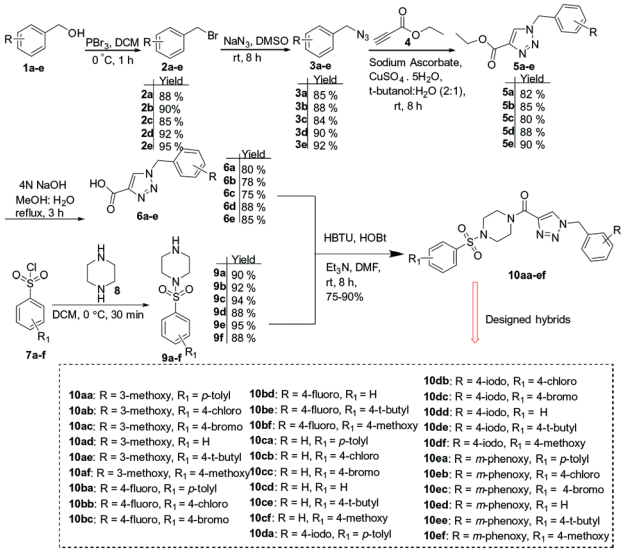

Scheme 1 Synthetic pathway for the preparation of sulfonyl piperazine-linked triazole conjugates (**10aa–ef**).

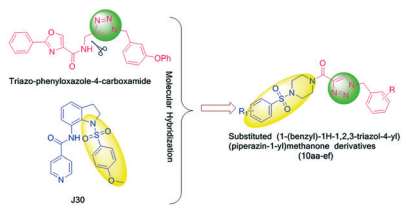

Fig. 2 Design of substituted (1-(benzyl)-1*H*-1,2,3-triazol-4-yl) (piperazin-1-yl)methanone conjugates (**10aa–ef**).

Evaluation of biological activity

***In vitro* cytotoxic activity.** All the as-synthesized compounds (**10aa–ef**) were evaluated for their *in vitro* anti-proliferative activity against the selected human cancer cell

lines of the breast (BT-474 and MCF-7 were procured from NCCS, Pune, India), cervical (HeLa were procured from NCCS, Pune, India), non-small cell lung (NCI-H460 were obtained from ATCC, USA) and human epidermal keratinocyte (HaCaT was a kind gift from Dr. Munia Ganguly, IGIB, New Delhi, India) by employing the 3-(4,5-dimethylthiazol-2-yl)-2,5-diphenyltetrazolium bromide (MTT) assay. Here, nocodazole was used as a control standard for comparing the cytotoxicity of the new chemical entities (NCEs). The IC_{50} (μM) values (concentration required to inhibit 50% of cancer cell growth) of tested compounds (**10aa–ef**) and reference (nocodazole) have been calculated in Microsoft Excel. The drug concentrations against the percent inhibition are plotted. The estimate of IC_{50} is by plotting x–y and fit the data with a straight line (linear regression). Using the linear ($y = mx + c$) equation on this graph, the IC_{50} value was determined and summarized in Table 1. Compound **10ec** was the most potent against BT-474 and HeLa with IC_{50} values of 0.99 ± 0.01 μM and 1.02 ± 0.18 μM, respectively. Moreover, **10ec** also showed to be active on MCF-7, NCI-H460 and HaCaT with IC_{50} values of 2.34 ± 0.05 μM, 4.88 ± 0.02 μM and 3.68 ± 0.19 μM, respectively. Among the series tested, compounds **10dc**, **10de** and **10ee** showed considerable cytotoxicity in all cancer cell lines.

It is evident from the IC_{50} values (Table 1) that the substitution of the R-group with *m*-phenoxy and R_1 is substituted with 4-bromo showed better cytotoxic activity among all derivatives. Furthermore, the removal of the substituent or introducing an electron-donating group (*p*-tolyl) at R_1; without changing the substitution pattern at R (*m*-phenoxy), progressively decreases the cytotoxicity (Fig. 3). Moreover, R_1 substituted with electron-withdrawing groups (4-Cl) showed considerable cytotoxicity. Replacing the *m*-phenoxy with 4-iodo at position R, and R_1 substituted with electron-withdrawing substituents (4-Cl and 4-Br) showed a detrimental effect on cytotoxicity. Considering the steric effect of the substituents such as Cl, Br, CH_3, OCH_3 and *t*-butyl, it can be seen that moderately bulkier Br, shows the highest potency among all of the other substitutions with less *A*-value or very high *A*-value, when R_1 = I or phenoxy (bulky groups). Therefore, further biological studies were carried out on one of the most potent compounds (**10ec**) from the series.

Tubulin polymerization assay. Tubulin is an important component of the cytoskeletal network and it is essential for the cellular functions mainly during mitosis. Tubulin is the target of several small molecules. Recently, several anti-proliferative compounds have been shown to function as tubulin polymerization inhibitors.[21,22] To investigate the

Table 1 Cytotoxicity of target compounds (**10aa–ef**) against selected human cancer cell lines (IC_{50} values in μM)[a]

Compound	[b]BT-474	[c]HeLa	[d]MCF-7	[e]NCI-H460	[f]HaCaT
10aa	>30	>30	>30	>30	>30
10ab	>30	>30	>30	>30	>30
10ac	>30	>30	>30	>30	>30
10ad	>30	>30	>30	>30	>30
10ae	>30	>30	>30	>30	>30
10af	>30	>30	>30	>30	>30
10ba	>30	>30	>30	>30	>30
10bb	>30	>30	>30	>30	>30
10bc	>30	>30	>30	>30	>30
10bd	>30	>30	>30	>30	>30
10be	>30	>30	>30	>30	>30
10bf	>30	>30	>30	>30	>30
10ca	>30	>30	>30	>30	>30
10cb	>30	>30	>30	>30	>30
10cc	>30	>30	>30	>30	>30
10cd	>30	>30	>30	>30	>30
10ce	>30	>30	>30	>30	>30
10cf	>30	>30	>30	>30	>30
10da	>30	>30	>30	>30	>30
10db	4.96 ± 0.13	5.74 ± 0.02	1.34 ± 0.04	2.25 ± 0.11	2.22 ± 0.71
10dc	2.33 ± 0.11	6.52 ± 0.01	2.73 ± 0.02	3.55 ± 0.18	2.48 ± 0.09
10dd	>30	>30	>30	>30	>30
10de	1.21 ± 0.17	3.58 ± 0.05	3.06 ± 0.18	1.42 ± 0.03	2.06 ± 0.05
10df	>30	>30	>30	>30	>30
10ea	>30	>30	>30	>30	>30
10eb	1.96 ± 0.14	8.61 ± 0.24	4.41 ± 0.24	5.68 ± 0.15	2.96 ± 0.05
10ec	0.99 ± 0.01	1.02 ± 0.18	2.34 ± 0.05	4.88 ± 0.02	3.68 ± 0.19
10ed	>30	>30	>30	>30	>30
10ee	3.89 ± 0.16	3.70 ± 0.02	3.28 ± 0.11	5.05 ± 0.18	4.34 ± 0.04
10ef	5.13 ± 0.15	3.72 ± 0.04	2.20 ± 0.19	8.20 ± 0.01	2.59 ± 0.17
Nocodazole[g]	0.87 ± 0.01	1.11 ± 0.08	1.76 ± 0.14	2.29 ± 0.05	1.19 ± 0.18

[a] 50% inhibitory concentration after 48 h of compounds treatment. [b] Breast cancer cells. [c] Cervical cancer cells. [d] Breast cancer cells. [e] Non-small cell lung cancer cells. [f] Human epidermal keratinocyte. [g] Reference compound. All the values are expressed as mean ± SEM in which each treatment was performed in triplicates.

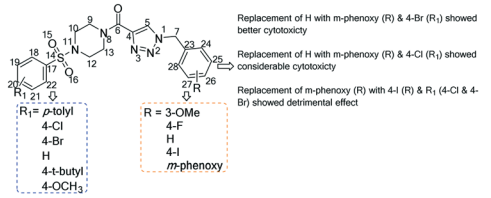

Fig. 3 SAR summary of sulfonyl piperazine integrated 1,2,3-triazole conjugates.

synthesized compound (compound **10ec**) used in the present study, which showed maximum cytotoxicity in the MTT assay and inhibited the cell cycle at the G2/M phase, was evaluated for its tubulin polymerization inhibitory activity in a cell-free *in vitro* assay. The assay was performed where nocodazole and paclitaxel were considered as standards and tubulin inhibition in the absence of test compounds was considered as control. The data obtained with standards and control was compared with the tubulin inhibition activity of the test compound. It was found that tubulin targeting ability of the test compound was moderate. Since it was moderate, some other additional targets may also be involved in controlling the cellular activity besides the tubulin polymerization inhibition. The details were shown in Fig. 4.

Immunohistochemistry assay to find the extent of tubulin polymerization inhibition. Results from the cell cycle experiments indicated that **10ec** is efficient in blocking the cell cycle at the G2/M phase. To check the possible mechanism of action of these molecules in exhibiting cytotoxicity among BT-474 cancer cells, immunohistochemistry assay was performed.[23]

BT-474 cells were treated with **10ec** at 2 μM concentration for 48 h. Combretastatin A-4 (CA-4), a known tubulin polymerization inhibitor used as a positive control. Confocal microscopic results suggested that untreated cancer cells displayed the normal distribution of microtubules, whereas cells treated with **10ec** and CA-4 compounds showed the disrupted microtubule organization as shown in Fig. 5.

Morphological observations using phase-contrast microscope. Morphological changes were observed using a phase-contrast microscope. As depicted in Fig. 6, the characteristic morphological changes such as cell wall deformation, shrinkage of cells, loss of cell–cell adhesion and reduction in the number of viable cells have been observed

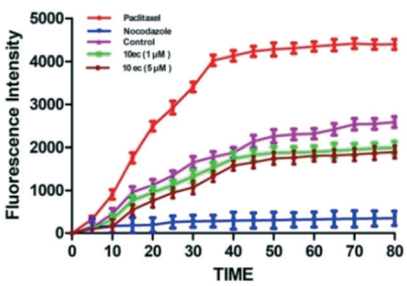

Fig. 4 Effect of compound **10ec** on tubulin polymerization.

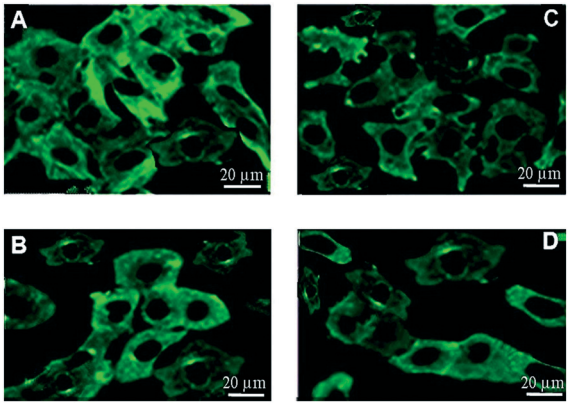

Fig. 5 BT-474 cells were treated with both CA-4 (control) and **10ec** for 48 h. A. Cells in the absence of **10ec** (untreated cells); B. Cells after the treatment of **10ec**; C. Cells in the absence of CA-4 (untreated cells); D. Cells after the treatment of CA-4.

in a concentration-dependent manner. However, morphological features were not present in control cells. After incubation of 48 h with compound **10ec**, the images were captured under a phase-contrast microscope.

Acridine orange/ethidium bromide (AO/EB) staining. To differentiate live, apoptotic and necrotic cells, the AO/EB staining assay was performed.

AO stains the nuclei in green that impregnate the intact cell membrane, whereas EB stains the nuclei in red that have lost membrane integrity. BT-474 cells were stained with AO/EB. Normal morphology was observed in the control cells. Fig. 7 clearly stated that morphological changes, such as non-uniform distribution of chromatin, chromatin condensation and membrane blebbing, were observed under a fluorescence microscope in dose-dependent manner, thus it indicates that compound had induced apoptosis in breast cancer cells.

DAPI staining. DAPI (4′,6-diamidino-2-phenylindole) is a blue fluorescent dye that binds firmly to the nucleus and distinguishes chromatin condensation or nuclear damage. DAPI stains the apoptotic nuclei as bright blue colour due to

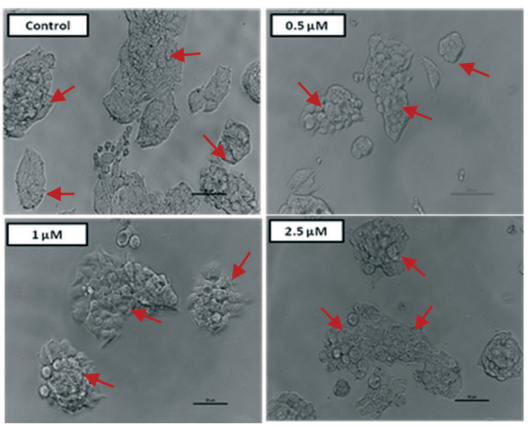

Fig. 6 BT-474 cells were treated with and without compound **10ec** at concentrations 0.5, 1 and 2.5 μM. Images were captured at 200× magnification. The scale bar in the image indicates 50 μm.

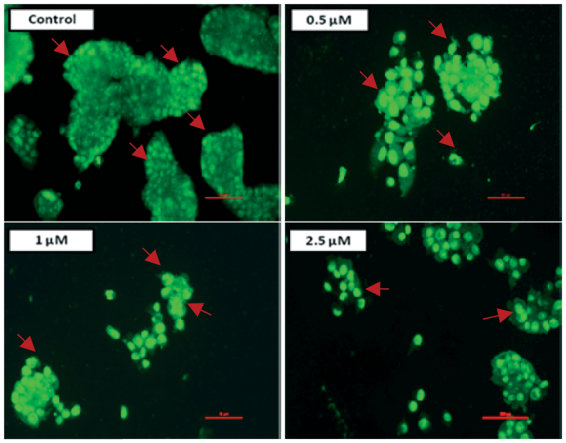

Fig. 7 AO/EB staining of compound **10ec**. Cells were treated with **10ec** in the concentration of 0.5, 1 and 2.5 μM and compared with control. Images were captured at 200× magnification. The red scale bar in the image indicates 50 μm.

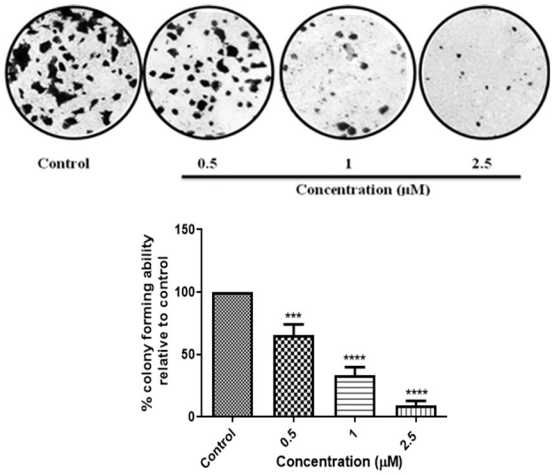

Fig. 9 Clonogenic assay was performed with compound **10ec**. BT-474 cells were treated with **10ec** in the concentration of 0.5, 1, 2.5 μM and compared with control (untreated cells).

the condensed nucleus and stains the live-cell nucleus as light blue. Hence, to observe the chromatin condensation or nuclear damage, DAPI staining was performed. It can be observed in Fig. 8 that the control cells were intact with normal morphology, while compound **10ec** treated cells showed horse shoe shaped nuclei, nuclear shrinkage, fragmented, pyknotic and chromatin condensation, these are the remarkable features of apoptosis.

Clonogenic growth inhibition assay. Disruption of the colony-forming ability in BT-474 cells by **10ec** was evaluated by the clonogenic assay, as shown in Fig. 9. We observed the formation of colonies in control, whereas after treatment with compound **10ec**, apparent reduction in the number of colonies was observed in a concentration-dependent manner (0.5, 1 and 2.5 μM). Hence, these results specify the importance of compound **10ec** in inhibiting colony formation in BT-474 cells. The total numbers of colonies were counted by a molecular imaging system (Vilber Fusion Fx software), and the values were represented as a percent colony-forming ability.

Cell cycle analysis. To understand the effect of **10ec** on cell cycle progression, the cell cycle analysis was performed using the propidium iodide staining method and the cells were treated with increasing concentrations (0.5, 1 and 2.5 μM) of **10ec**. It can be seen in Fig. 10 that a significant increase in the population of cells at sub G1 (from 4.06% to 11.30%) and G2/M phase (from 19.35% to 63.41%) happen as compared to the control cells. However, the moderate accumulation of cells in the S phase (from 2.22% to 5.57%) and extreme decrement of cells in the G0/G1 phase (60.53% to 9.09%) was also observed. Collectively, these results indicate that compound **10ec** induces blockade at the sub-G1 and G2/M phase.

Effect on mitochondrial membrane potential ($\Delta\Psi m$). The effect of compound **10ec** on the mitochondrial membrane potential ($\Delta\Psi m$) was determined using the JC-1 staining method. JC-1 is a lipophilic cationic dye. Normal polarised

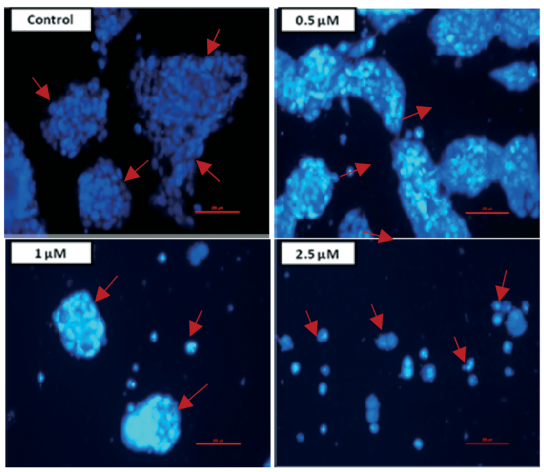

Fig. 8 DAPI staining of compound **10ec**. BT-474 cells were treated with **10ec** in the concentration of 0.5, 1, 2.5 μM and compared with control (untreated cells). Images were captured at 200× magnification. Red scale bar in the image indicates 50 μm.

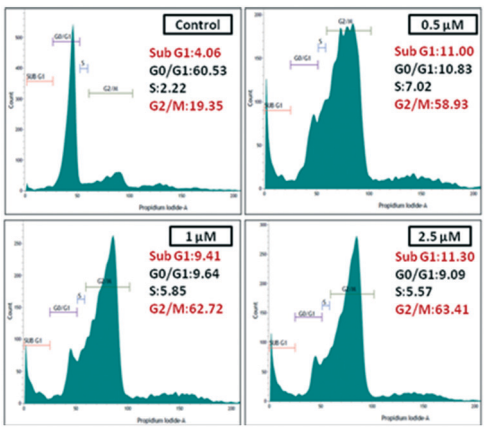

Fig. 10 Effect of **10ec** on the cell cycle progression of BT-474 cells. Cells were treated with **10ec** (0.5, 1 and 2.5 μM) and cell cycle analysis was performed by the flow cytometric analysis using PI staining.

mitochondria stain red due to the formation of JC-1 oligomers, whereas depolarised mitochondria stain green due to the formation of J-monomers. Cells were treated with increasing concentrations (0.5, 1 and 2.5 μM) of compound **10ec** for 48 h and mitochondrial membrane potential was observed with respect to the control. The flow cytometric analysis clearly demonstrates that increase in the depolarized cell population (P2) from control (0.48%) to 50.48% (0.5 μM), 61.44% (1 μM) and 89.84% (2.5 μM), respectively in a concentration-dependent manner (Fig. 11). Thus, compound **10ec** triggered the depolarisation of $\Delta\Psi m$ which indicates that cytotoxic effect associated with mitochondria.

Annexin V-Alexa fluor 488/PI assay. To quantify the apoptotic cell death induced by compound **10ec**, the Annexin V-Alexa fluor 488/propidium iodide staining assay was used. Cells were treated with 0.5, 1 and 2.5 μM of **10ec** for 48 h were stained with Annexin V-Alexa fluor 488/propidium iodide, and samples were analysed using flow cytometry.

Annexin assay expedites the detection of necrotic cells (Q1-UL; AV−/PI+), live cells (Q2-LL; AV−/PI−), early apoptotic cells (Q3-LR; AV+/PI), and late apoptotic cells (Q1-UR; AV+/PI+). Therefore, compound **10ec** induces apoptosis in a concentration-dependent manner in comparison to the control, as shown in Fig. 12.

***In silico* computational studies.** Lipinski parameters (TPSA, NRotB, log*P*, *n*OH–NH, *n*O–N, molecular weight and number of violations) can be assessed using molinspiration online property calculation tool kit.[24] The solubility and drug score values were predicted by using molsoft software[25] and the results are depicted in Table S2 in the ESI† file. Molecules likely to be having TPSA ≤ 140 Å^2, NRotB ≤ 10, milog*P* value must be in the range of −0.4 to 5, clog*S* < −4, molecular weight ≤ 500, hydrogen bond donor sites (*n*OHNH) ≤ 5 and hydrogen bond acceptor sites (*n*ON) ≤ 10. On this basis, all the synthesized analogues were found to be within the acceptable range and are anticipated to have good oral absorption. It is noteworthy that analyzed compounds (**10db**, **10dc**, **10de**, **10eb**, **10ec** and **10ef**) have one or zero violations except **10ee**. Moreover, compounds that violated Lipinski's rules either have a molecular weight larger than 500 or showed log*P* > 5 (octanol–water partition coefficients). The prediction of physicochemical parameters for good bioavailability can be useful for the design of safe and effective compounds at the advanced stages of the drug discovery process.

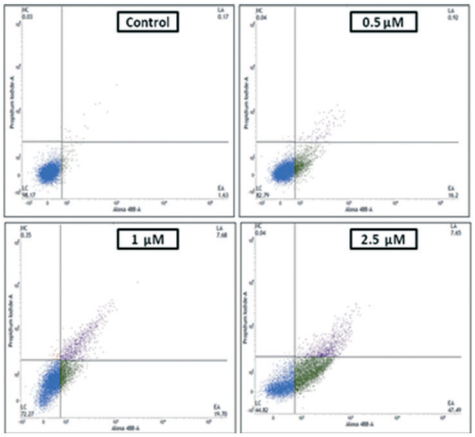

Fig. 12 Effect of compound **10ec** on the apoptotic cell death in BT-474 cells. The compound **10ec** treated cells were stained with Annexin V-Alexa fluor 488/propidium iodide and analysed for apoptosis using a flow cytometer. The 10 000 cells from each sample were analysed *via* flow cytometry.

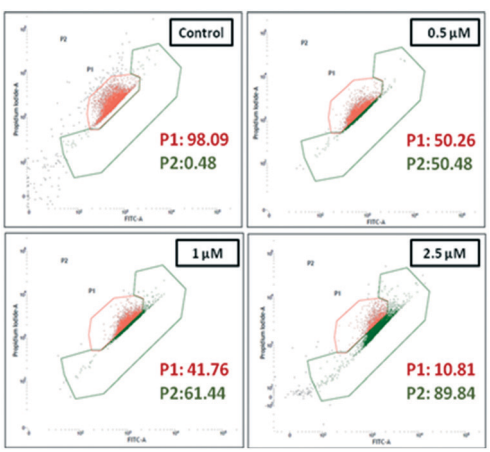

Fig. 11 Effect on compound **10ec** on mitochondrial membrane potential. BT-474 cells were treated **10ec** in the concentration of 0.5, 1, 2.5 μM and compared with control (untreated cells).

Molecular docking studies. To understand the binding view and the nature of contacts with tubulin protein (PDB ID: 3E22),[26] we have performed molecular docking studies on the most active compound **10ec** by employing the GLIDE module of Schrödinger 2017-1 (ref. 27) software. The molecular docking results for compound **10ec** are depicted in Table S3 in the ESI† file. Compound **10ec** has made three hydrogen

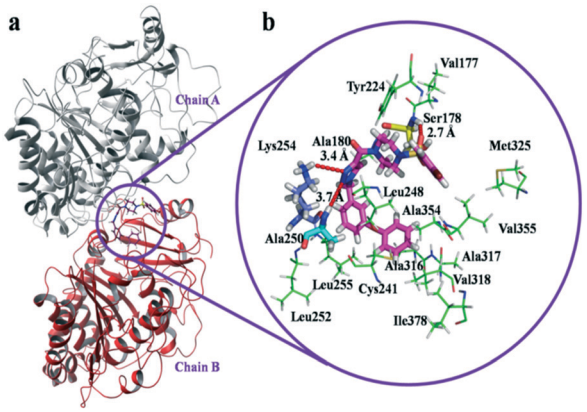

Fig. 13 a) Molecular docking view of the compound **10ec** (maroon color ball and stick) and b) its ligand–protein interactions in the active site of α/β-tubulin (PDB ID: 3E22). The red dashed line represents a hydrogen bond. The atom colors for all amino acids are as follows: for all amino acids residues [nitrogen (dark blue), oxygen (red) and hydrogen (white)], Ser178 [carbon (yellow)], Ala250 [carbon (cyan)], Lys254 [carbon (light blue)], Cys241 and Met325 [carbon (green), sulphur (pale yellow)], for all other amino acids residues [carbon (green)].

bond contacts with the binding site residues Ser178, Ala250 and Lys254. The sulfonyl group of compound **10ec** has established strong hydrogen bond interaction with Ser178 (*d* = 2.7 Å). The triazole moiety has formed two hydrogen bond interactions with binding site residues Ala250 and Lys254 with a distance of 3.7 Å and 3.4 Å respectively. In addition, compound **10ec** showed hydrophobic interactions that stabilize the compound in the binding pocket of α/β-tubulin. As shown in Fig. 13, compound **10ec** has shared hydrophobic contacts with Val177, Ala180, Tyr224, Cys241, Leu248, Ala250, Leu252, Leu255, Ala316, Ala317, Val318, Met325, Ala354, Val355 and Ile378 of α/β-tubulin. Moreover, compound **10ec** was well lodged in the binding site interphase of α/β-tubulin and established a number of interactions with its key residues. From the rational justification of docking studies, we understood that compound **10ec** has the good tubulin polymerization inhibitory activity and obtained many key instructions for future design and synthesis of potential tubulin polymerization inhibitors.

Conclusion

In the current study a series of substituted (1-(benzyl)-1*H*-1,2,3-triazol-4-yl)(piperazin-1-yl)methanone derivatives were synthesized and evaluated for their *in vitro* cytotoxic potential against a selected panel of human cancer cell lines such as BT-474 (breast), HeLa (cervical), MCF-7 (breast), NCI-H460 (non-small cell lung cancer) and HaCaT (human epidermal keratinocytes) using the MTT assay. Compound **10ec** showed potent cytotoxicity on the BT-474 cancer cell line with an IC_{50} value of 0.99 ± 0.01 μM. The flow cytometric analysis indicated that compound **10ec** inhibits the cell cycle at sub-G1 and G2/M phase. Compound **10ec** could also effectively inhibit tubulin polymerization with an increase in the concentration. Moreover, biological studies such as phase contrast microscope, acridine orange/ethidium bromide (AO/EB), DAPI, annexin V-FITC assay suggested that compound **10ec** induced morphological changes and cell proliferation is inhibited through the induction of apoptosis in BT-474 cell line. Molecular modelling studies revealed that compound **10ec** interacted with the tubulin *via* colchicine binding site. Overall, the current studies suggest that compound **10ec** could be a potential lead for the development of a library of compounds, and further modifications in the structure may produce newer anticancer agents.

Conflicts of interest

There is no conflict of interest to declare.

Acknowledgements

The authors thank and acknowledge the Department of Pharmaceuticals, Ministry of Chemicals & Fertilizers and CSIR-Indian Institute of Chemical Technology, Hyderabad, India for providing funds, Scientific and Instrumental support (IICT Comm. No. IICT/Pubs./2020/217).

References

1 (*a*) J. F. Billing and U. J. Nilsson, *J. Org. Chem.*, 2005, **70**, 4847–4850; (*b*) K. D. Bodine, D. Y. Gin and M. S. Gin, *Org. Lett.*, 2005, **7**, 4479–4482; (*c*) Z. Zhou and C. J. Fahrni, *J. Am. Chem. Soc.*, 2004, **126**, 8862–8863; (*d*) T. Jin, S. Kamijo and Y. Yamamoto, *Eur. J. Org. Chem.*, 2004, **2004**, 3789–3791; (*e*) K. D. Bodine, D. Y. Gin and M. S. Gin, *J. Am. Chem. Soc.*, 2004, **126**, 1638–1639; (*f*) T. S. Seo, Z. Li, H. Ruparel and J. Ju, *J. Org. Chem.*, 2003, **68**, 609–612.

2 (*a*) P. L. Golas, N. V. Tsarevsky, B. S. Sumerlin and K. Matyjaszewski, *Macromolecules*, 2006, **39**, 6451–6457; (*b*) D. D. Diaz, S. Punna, P. Holzer, A. K. McPherson, K. B. Sharpless, V. Fokin and M. G. Finn, *J. Polym. Sci., Part A: Polym. Chem.*, 2004, **42**, 4392–4403; (*c*) P. Wu, A. K. Feldman, A. K. Nugent, C. J. Hawker, A. Scheel, B. Voit, J. Pyun, J. M. J. Fréchet, K. B. Sharpless and V. V. Fokin, *Angew. Chem., Int. Ed.*, 2004, **43**, 3928–3932.

3 (*a*) M. J. Genin, D. A. Allwine, D. J. Anderson, M. R. Barbachyn, D. E. Emmert, S. A. Garmon, D. R. Graber, K. C. Grega, J. B. Hester, D. K. Hutchinson, J. Morris, R. D. Reischer, D. Stper and B. H. Yagi, *J. Med. Chem.*, 2000, **43**, 953–970; (*b*) R. Alvarez, S. Velazquez, A. San-Felix, S. Aquaro, E. De Clercq, C.-F. Perno, A. Karlsson, J. Balzarini and M. J. Camarasa, *J. Med. Chem.*, 1994, **37**, 4185–4194.

4 S. Lober, P. Rodriguez-Loaiza and P. Gmeiner, *Org. Lett.*, 2003, **5**, 1753–1755.

5 (*a*) A. Kamal, S. Prabhakar, M. J. Ramaiah, P. V. Reddy, C. R. Reddy, A. Mallareddy, N. Shankaraiah, T. L. N. Reddy, S. N. C. V. L. Pushpavalli and M. P. Bhadra, *Eur. J. Med. Chem.*, 2011, **46**, 3820–3831; (*b*) K. D. Thomas, A. V. Adhikari, I. H. Chowdhury, E. Sumesh and N. K. Pal, *Eur. J. Med. Chem.*, 2011, **46**, 2503–2512; (*c*) R. He, Y. Chen, Y. Chen, A. V. Ougolkov, J. S. Zhang, D. N. Savoy, D. D. Billadeau and A. P. Kozikowski, *J. Med. Chem.*, 2010, **53**, 1347–1356; (*d*) A. Kamal, N. Shankaraiah, V. Devaiah, K. Laxma Reddy, A. Juvekar, S. Sen, N. Kurianb and S. Zingdeb, *Bioorg. Med. Chem. Lett.*, 2008, **18**, 1468–1473.

6 J. L. Kelley, C. S. Koble, R. G. Davis, E. W. McLean, F. E. Soroko and B. R. Cooper, *J. Med. Chem.*, 1995, **38**, 4131–4134.

7 (*a*) M. J. Genin, D. A. Allwine, D. J. Anderson, M. R. Barbachyn, D. E. Emmert, S. A. Garmon, D. R. Graber, K. C. Grega, J. B. Hester, D. K. Hutchinson, J. Morris, R. J. Reischer, C. W. Ford, G. E. Zurenko, J. C. Hamel, R. D. Schaadt, D. Stapert and B. H. Yagi, *J. Med. Chem.*, 2000, **43**, 953–970; (*b*) G. A. Nilkanth, S. P. Vandana, N. M. Nripendra, A. Kumar, K. S. Praveen, A. Sharma and K. B. Manoj, *Bioorg. Med. Chem. Lett.*, 2009, **19**, 759–763.

8 D. R. Buckle, D. J. Outred, C. J. M. Rockell, H. Smith and B. A. Spicer, *J. Med. Chem.*, 1983, **26**, 251–254.

9 D. R. Buckle and C. J. M. Rockell, *J. Chem. Soc., Perkin Trans. 1*, 1982, **1**, 627–630.

10 R. Alvarez, S. Velazquez, A. San-Felix, S. Aquaro, E. De Clercq, C.-F. Perno, A. Karlsson, J. Balzarini and M. J. Camarasa, *J. Med. Chem.*, 1994, **37**, 4185–4194.

11 (*a*) G. Biagi, G. Dell Omodarme, M. Ferretti, I. Giorgi, O. Livi and V. Scartoni, *Farmaco*, 1990, **45**, 1181–1192; (*b*) G. Biagi, O. Livi, V. Scartoni, A. Lucacchini and M. R. Mazzoni, *Farmaco*, 1986, **41**, 597–610.

12 (*a*) H. C. Kolb and K. B. Sharpless, *Drug Discovery Today*, 2003, **8**, 1128–1137; (*b*) G. S. Mani, K. Donthiboina, S. P. Shaik, N. Shankaraiah and A. Kamal, *RSC Adv.*, 2019, **9**, 27021–27031.

13 P. Thirumurugan, D. Matosiuk and K. Jozwiak, *Chem. Rev.*, 2013, **113**, 4905–4979.

14 (*a*) H. K. Amol, V. S. Pravin, H. K. Atul, K. P. Sharad, B. S. Bapurao and S. S. Murlidhar, *Eur. J. Med. Chem.*, 2010, **45**, 3142–3146; (*b*) C. Hong, Z. Song, W. Xiaochen, T. Xiaowei, Z. Ming, L. Yanling, C. Liting, L. Jing, L. Yongfeng, L. Dailin, Z. Shi and L. Tan, *Eur. J. Med. Chem.*, 2011, **46**, 4709–4714.

15 C. Avijeet, A. Amy and G. Charles, *J. Biol. Chem.*, 2014, **289**, 2978–2991.

16 (*a*) C. Wasylyk, H. Zheng, C. Castell, L. Debussche, M.-C. Multon and B. Wasylyk, *Cancer Res.*, 2005, **68**, 1275–1283; (*b*) A. Chopra, A. Anderson and C. Giardina, *J. Biol. Chem.*, 2014, **289**, 2978–2991.

17 N. M. O'Boyle, G. Ana, P. M. Kelly, S. M. Nathwani, S. Noorani, D. Fayne, S. A. Bright, B. Twamley, D. M. Zisterer and M. J. Meegana, *Org. Biomol. Chem.*, 2019, **17**, 6184–6200.

18 C. Avijeet, A. Amy and G. Charles, *J. Biol. Chem.*, 2014, **289**, 2978–2991.

19 J. Xie and C. T. Seto, *Bioorg. Med. Chem.*, 2007, **15**, 458–473.

20 C. Jadala, M. Sathish, P. Anchi, R. Tokala, U. J. Lakshmi, V. G. Reddy, N. Shankaraiah, C. Godugu and A. Kamal, *ChemMedChem*, 2019, **14**, 2052–2060.

21 P. V. Sri Ramya, S. Angapelly, L. Guntuku, C. S. Digwal, B. N. Babu, V. G. M. Naidu and A. Kamal, *Eur. J. Med. Chem.*, 2017, **127**, 100–114.

22 J. Xi, X. Zhu, Y. Feng, N. Huang, G. Luo, Y. Mao, X. Han, W. Tian, G. Wang, X. Han, R. Luo, Z. Huang and J. An, *Mol. Cancer Res.*, 2013, **11**, 856–864.

23 (*a*) M. Borowiak, W. Nahaboo, M. Reynders, K. Nekolla, P. Jalinot, J. Hasserodt, M. Rehberg, M. Delattre, S. Zahler, A. Vollmar, D. Trauner and O. Thorn-Seshold, *Cell*, 2015, **162**, 403–411; (*b*) M. Cazales, R. Boutros, M.-C. Brezak, S. Chaumeron, G. Prevost and B. Ducommun, *Mol. Cancer Ther.*, 2007, **6**, 318–325; (*c*) C. Stengel, S. P. Newman, M. P. Leese, B. V. L. Potter, M. J. Reed and A. Purohit, *Br. J. Cancer*, 2010, **102**, 316–324.

24 P. Ertl, Calculation of Molecular Properties and Bioactivity Score, Available online: http://www.molinspiration.com (accessed on 31 January 2012).

25 Molsoft L. L. C., Drug-Likeness and molecular property prediction, http://molsoft.com/mprop/.

26 A. Cormier, M. Marchand, R. B. Ravelli, M. Knossow and B. Gigant, *EMBO Rep.*, 2008, **9**, 1101–1106.

27 Schrödinger, *Schrödinger Suite 2017–1*, LLC, New York, 2017.

